Land-Sea Contrast of Nearshore Wind Conditions: Case Study in Mutsu-Ogawara

Konagaya, Mizuki ; Ohsawa, Teruo ; Inoue, Takaya ; Mito, Toshinari ; Kato, Hideki ; Kawamoto, Kazuhiro

(Citation)
SOLA,17:234-238

(Issue Date)
2021

(Resource Type)
journal article

(Version)
Version of Record

Land–Sea Contrast of Nearshore Wind Conditions: Case Study in Mutsu-Ogawara

Mizuki Konagaya[1, 2], Teruo Ohsawa[2], Takaya Inoue[2],
Toshinari Mito[1], Hideki Kato[3], and Kazuhiro Kawamoto[4]
[1]*Rera Tech Inc.*, *Hyogo*, *Japan*
[2]*Graduate School of Maritime Sciences*, *Kobe University*, *Hyogo*, *Japan*
[3]*E&E Solutions Inc.*, *Tokyo*, *Japan*
[4]*Mutsuogawara Port Offshore Windpower Development*, *Aomori*, *Japan*

Abstract

To develop offshore wind energy, we investigated nearshore wind conditions, notably the land–sea contrast, using the coastal area of Mutsu-Ogawara, Aomori Prefecture as a case study. We found that wind conditions were substantially different between onshore (MT-A1) and offshore (MT-B) sites, even when the latter were only 1.5 km apart. The mean wind speed at 55 m above sea level at MT-B was higher than that at the onshore site by up to 20% monthly and 12% annually. For winds from the landward side, the Iref value (turbulence intensity at a mean wind speed of 15 m/s) at MT-B was 37% lower than that at MT-A1. Because such high wind speeds and low turbulence conditions are preferable for the operation of wind turbines, an offshore wind farm would have advantageous wind conditions, even if placed close to the coastline. Moreover, we found that the land–sea contrast is caused not only by mechanical factors, such as roughness length, but also by thermodynamic factors such as seasonal variations of atmospheric stability over land and sea.

(**Citation**: Konagaya, M., T. Ohsawa, T. Inoue, T. Mito, H. Kato, and K. Kawamoto, 2021: Land–sea contrast of nearshore wind conditions: Case study in Mutsu-Ogawara. *SOLA*, **17**, 234−238, doi:10.2151/sola.2021-041.)

1. Introduction

To develop an offshore wind farm, it is important to precisely understand the wind conditions at the candidate site. In Europe, offshore wind farms are mostly installed far from coastlines; hence, they are minimally affected by land (Rodrigues et al. 2015). In contrast, because of the surrounding deep seas, the installation of offshore wind farms in Japan has started in nearshore shallow waters (Sayigh and Milborrow 2020), which is greatly affected by the land. Therefore, a reliable method for wind resource assessments, that is applicable to nearshore areas, is required for wind energy development in Japan.

For offshore wind resource assessments in Japan's coastal waters, the first task is to clarify the characteristics of nearshore wind conditions, especially for areas within several kilometers of a coastline. It is necessary to determine the space-time structure and mechanism of wind speed and turbulence distributions, which are controlled by factors such as land–sea breeze circulations, internal boundary layers, land–sea differences in surface roughness, and atmospheric stability (Hsu 1988; Nassif et al. 2020).

However, it is difficult to observe offshore wind conditions at the wind turbine hub height, which is more than 100 m. Thus, studies that examine the differences in wind speed between onshore and offshore sites located in a particular coastal area, such as Nagai et al. (2003) and Shimada et al. (2018), are very limited in Japan. Moreover, there are very few comparative studies that investigate wind shear and turbulence intensity differences between onshore and offshore sites, which are important parameters for wind turbine design; one such study was conducted by SethuRaman and Raynor (1980). Our research aims to clarify the characteristics of nearshore wind conditions, especially their land–sea contrast, using in-situ observation data from two onshore and offshore meteorological masts (met masts) and a vertical LiDAR (light detection and ranging) in Mutsu-Ogawara, Aomori Prefecture.

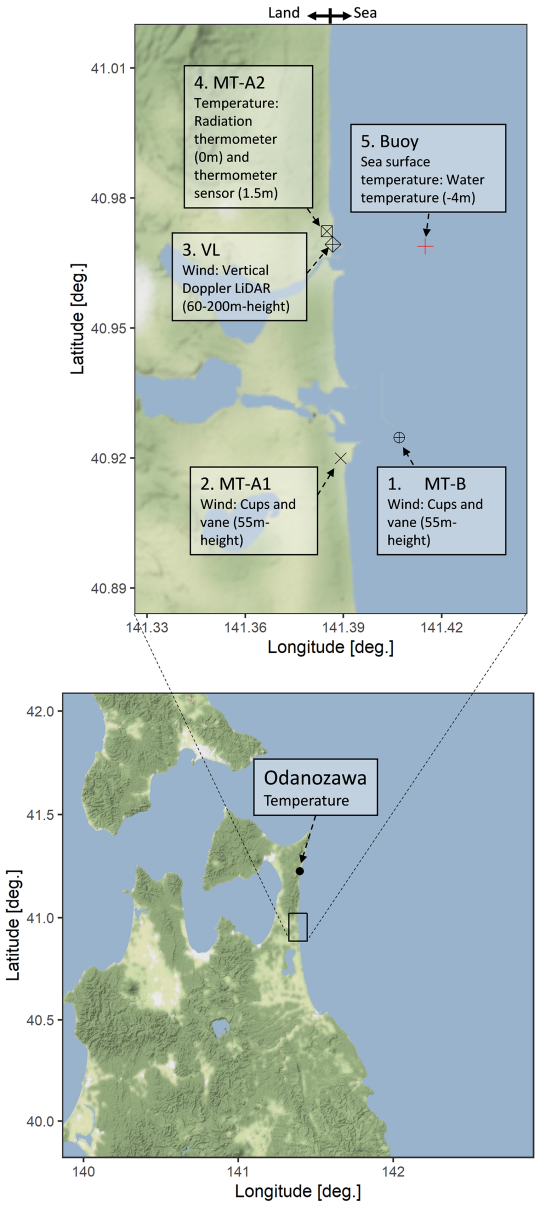

Fig. 1. Locations of the study area, observation sites, and outline of the measurements at each site.

Corresponding author: Mizuki Konagaya, Rera Tech Inc., 5-1-1 Fukaeminami-machi, Higashinada-ku, Kobe 658-0022, Japan. E-mail: m.konagaya@rera-tech.co.jp.

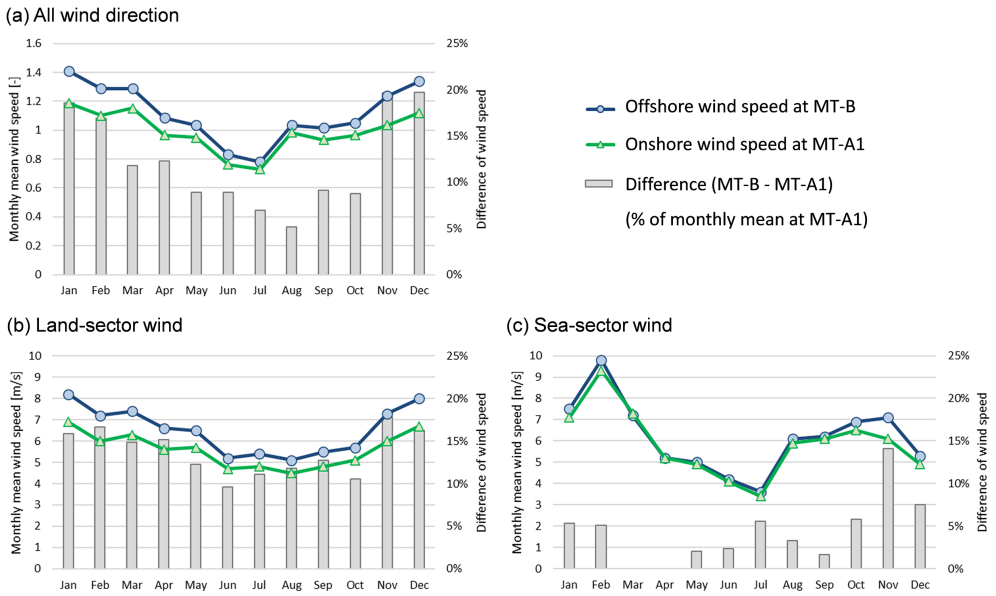

Fig. 2. Monthly mean wind speeds at 55 m ASL at the offshore site MT-B, the onshore site MT-A1, and their differences for April 2017 to March 2018; (a) wind speeds for all wind directions which is normalized by the annual mean wind speed at MT-A1. (b) the monthly mean wind speed in absolute values for the land-sector, and (c) the same as (b) but for the sea-sector.

2. Observation data

We set up several land and sea observation sites around the Mutsu-Ogawara Port in Rokkasho Village. The location of the study area, observation sites, and outline of the measurements at each site are shown in Fig. 1.

The analysis period was from April 2017 to June 2018. Data availability was sufficient for the analyses in this study, and more than 95.2% of the collected data could be used.

2.1 Onshore and offshore met masts

Wind speed and direction were measured with 3-cup anemometers and vanes on the met mast at onshore (MT-A1) and offshore (MT-B) sites. Measurements at a height of 55 m above sea level (ASL) were used for the analysis as representative data of offshore wind conditions. The onshore met mast at MT-A1 was approximately 1.5 km from the met mast at MT-B at 55 m ASL (elevation of 5 m + 50 m above ground level (AGL)). The measurements at 55 m were used as representative data for onshore wind conditions.

2.2 Wind profile from vertical Doppler LiDAR

Vertical profiles of wind speed and direction were measured using a vertical Doppler LiDAR installed at site VL near the coastline. The LiDAR instrument was Mitsubishi Electric's DIABREZZA (Kotake et al. 2016). The LiDAR was installed on the rooftop of a building at a height of 10 m ASL (elevation + AGL); the wind speed and direction measurements at 60−200 m ASL were used in the analysis.

2.3 Temperature observations on land and sea surfaces

At the buoy site, approximately 3 km off the coastline, sea surface temperature (SST) observations are routinely conducted using a mooring buoy (Shima 2016). This study used SST data from a depth of 4 m. The land surface temperature and air temperature were measured on the beach at MT-A2. These measurements were used as onshore temperature data for the analysis. However, due to their limited observation period, the temperature data measured at the Odanosawa station of the Japan Meteorological Agency, about 30 km to the north, was also used.

3. Differences between onshore and offshore wind conditions

The mean wind speed and turbulence intensity are two of the most important parameters for evaluating the business viability of a wind farm and determining the design strength of a wind turbine; thus, the parameters between onshore and offshore sites are discussed in this section. The comparison is made separately for sea-sector winds (wind direction: 0−180°) and land-sector winds (180−360°), with the sector separation being defined by the wind direction at the offshore site MT-B.

3.1 Wind speed

Figure 2 shows the monthly mean wind speeds, and Figs. S1−S3 in the supplementary materials illustrate the monthly and annual wind roses at 55 m ASL at MT-B. The wind roses revealed that the predominant wind direction is westerly or west-northwest, which means that most of the winds blow from the land, except in warm season, when easterly wind blows such as "Yamase" (Kanno 1997).

Although MT-B and MT-A1 are only 1.5 km apart, wind speed is clearly higher at MT-B. The annual mean wind speed at MT-B was higher than that at MT-A1 by 12%, and the monthly mean wind speed reached a maximum of 20% in December. In Figs. 2(b) and (c), the monthly mean wind speed is depicted separately for the land and sea-sector winds. It is clear that the land-sector winds lead to greater differences in wind speed between onshore and offshore sites than sea-sector winds. The wind speed differences between MT-B and MT-A1 were mainly due to mechanical effects such as the land–sea contrast of roughness length and the windbreak zone on the windward side. Westerly winds that decelerated because of a high roughness length and the windbreak zone at MT-A1, accelerated over the sea, reaching MT-B with 10%−20% greater speeds.

In contrast with the land-sector wind, the sea-sector wind exhibited much smaller differences between onshore and offshore sites. This result indicates that the offshore wind profile is advected directly to the onshore site MT-A1. However, it was also observed that the onshore–offshore wind speed differences became larger in the cold season, exhibiting the maximum difference in November. This was probably due to thermodynamic effects on the internal boundary layer, which are discussed in Section 4.

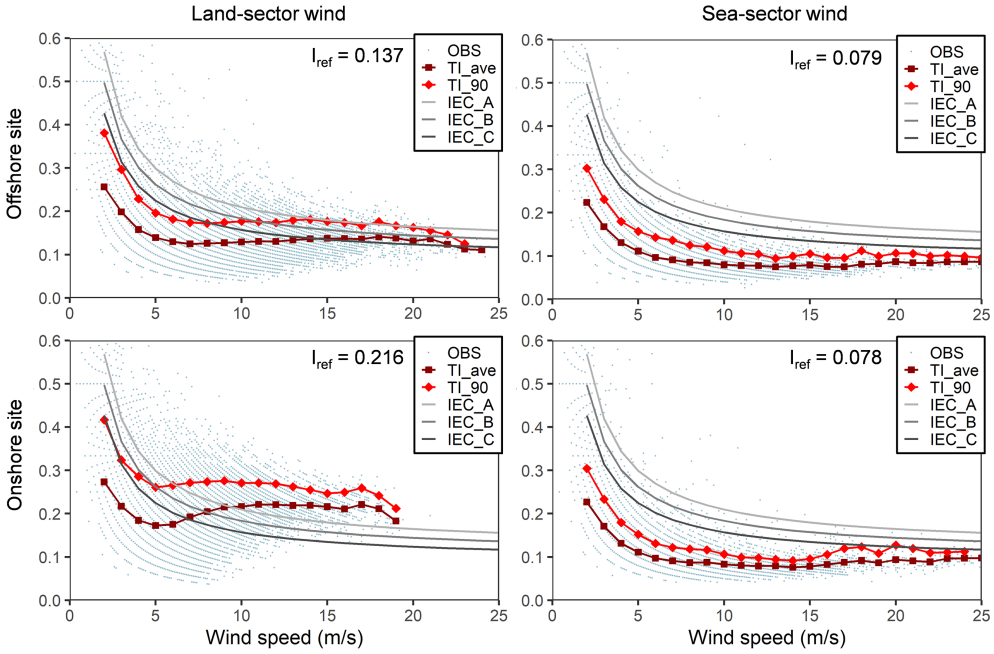

Fig. 3. Turbulence intensity at the offshore site MT-B (upper) and the onshore site MT-A1 (lower). Figures on the left and right are for the land-sector wind and sea-sector wind, respectively. The curves labeled as IEC (A: Higher turbulence – C: Lower turbulence) indicate the wind turbine categories for turbulence characteristics designated by IEC 61400-1 (2019) and I_{ref} represents the reference value of turbulence intensity at the wind speed of 15 m/s.

3.2 Turbulence intensity

Because turbulence substantially impacts the fatigue load of wind turbines, it is necessary to understand the turbulence intensity at the planned site. The turbulence intensity I is obtained by dividing the standard deviation σ by the mean wind speed $\bar{u}$ in 10 minutes in IEC 61400-1 (2019), which relates design requirements of wind turbines, as follows:

$$I = \frac{\sigma}{\bar{u}}, \quad \sigma = \sqrt{\frac{1}{n}\sum_{i=1}^{n}(u_i - \bar{u})^2} \tag{1}$$

where u_i is the instantaneous wind speed (sampling rate of 1 Hz) and n is the number of data points in 10 minutes. The average and 90-percentile values calculated for wind speed bin are used for wind turbine design.

Figure 3 shows the turbulence intensity measured at the offshore site MT-B and onshore site MT-A1 for the land and sea-sector winds. Firstly, when looking at the turbulence intensity at MT-A1, a large difference is found between both sectors. This means that effects of the surface roughness contain large hysteresis. MT-B, however, shows less sector differences, which indicates small roughness of the sea surface between the two sites weakened the turbulence advected from the land sector. Thus, for the land-sector wind, the turbulence intensity at MT-B was lower than that at MT-A1 as a whole. The I_{ref} values (turbulence intensity at a wind speed of 15 m/s) were 0.137 and 0.216 for the offshore and onshore sites, respectively, and the I_{ref} was 37% lower offshore compared to onshore. To the west of MT-A1, there is a windbreak zone covered by trees with heights of 10 m or more, which was likely the main cause of high turbulence intensity at the onshore site. It should be noted that the high wind turbulence drastically reduced at a distance of only 1.5 km to the offshore site.

In contrast, for the sea-sector wind, the offshore and onshore sites exhibited similar distributions of the mean and 90-percentile values, which were much smaller than those for the land-sector winds. In addition, both I_{ref} values were almost the same (offshore: 0.079; onshore: 0.078). These results indicate the possibility of estimating the offshore turbulence intensity from onshore measurements when wind blows from the sea-sector, although this is impossible for land-sector winds.

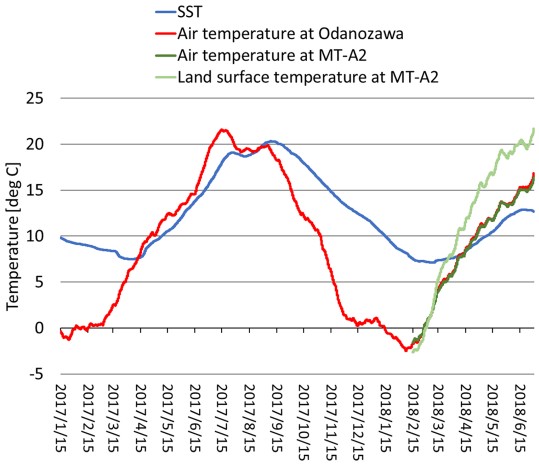

Fig. 4. Four temperature time series for January 2017−May 2018 in the study area—sea surface temperature at buoy (blue), air temperature at Odanosawa JMA observation station (red), air temperature (dark green) and land surface temperature (pale green) at site MT-A2. The four lines show 30-day moving averages for each temperature.

4. Discussion in terms of atmospheric stability

4.1 Warm and cold seasons

Figure 4 shows four temperature time series in the study area from January 2017 to May 2018. The air temperature at Odanosawa, approximately 30 km north of the site MT-A2, was used because the temperature measurements at MT-A2 were only available for approximately five months.

The SST exhibited a smaller seasonal variation than the air temperature on land, as well as the land surface temperature (Fig. 4). This is generally due to the difference in heat capacity between the land and sea. The seasonal mean atmospheric stabilities over land and sea can be estimated from the graph. From April to

Table 1. Seasonal variations of atmospheric stability at onshore and offshore sites.

	Warm season (April to August)	Cold season (September to March)
Onshore site	Unstable	Stable
Offshore site	Stable (or neutral)	Unstable

August, the air temperature on land was slightly higher than the SST. Assuming that air temperature does not change significantly between the onshore and offshore sites owing to the short distance, the above situation meant that stable (or neutral) conditions prevailed over the sea during this period. In April and May 2018, the land surface temperature was higher than the air temperature. This means that unstable conditions prevailed over the land during this period. Conversely, during September to March, the air temperature became colder than the SST and strong unstable conditions prevailed over the sea. Meanwhile, the difference between air and land surface temperatures observed in February and March 2018 indicated that stable conditions (air temperature > land surface temperature) prevailed over the land during this period.

The estimated seasonal mean atmospheric stability is thus summarized in Table 1. Here, the periods from April to August and from September to March are referred to as "warm season" and "cold season," respectively.

4.2 Vertical wind shear

Figure 5 shows mean wind speed profiles for June 2017−May 2018, measured using LiDAR at the onshore site VL, which are displayed separately for the land and sea-sector winds. The wind shear is expressed by the exponent α and the reciprocal number N ($= 1/\alpha$), defined as,

$$V(z) = V(z_r) \cdot \left(\frac{z}{z_r} \right)^{\alpha} \tag{2}$$

where $V(z)$ is the wind speed at height z and z_r is the reference height (IEC 61400-1, 2019). Comparing the wind shear between the land and sea-sector winds, it was obvious that land-sector wind exhibited greater wind shear than sea-sector wind. This result can be explained in terms of mechanical factors, such as the difference in the roughness length between the land and sea surfaces. In addition, the windbreak forest canopy likely affected the land-sector wind, especially in the lower part of the profile, adding to the vertical shear.

Furthermore, differences in wind shear were compared between the warm and cold seasons. The sea-sector wind was found to have a lower shear in the cold season (N = 11.31) than in the warm season (N = 6.75). This high seasonal difference indicates that the vertical shear of the sea-sector wind largely depended on atmospheric stability over the sea. Considering the seasonal variations in atmospheric stability listed in Table 1, the lower shear in the cold season was caused by unstable stratification, and the relatively higher shear in the warm season was due to neutral to stable conditions. In contrast, the land-sector wind showed almost the same value of N for the warm (N = 2.86) and cold seasons (N = 2.89), despite the substantial difference in atmospheric stability between the two seasons (shown in Subsection 4.1). These results indicate that the vertical shear of the land-sector wind is governed by mechanical effects, such as surface roughness and canopy, rather than thermodynamic effects. This is probably due to a large friction velocity u^* over rough surface, which leads to a larger Obukhov length L, that is, a neutral stratification.

4.3 Turbulence intensity

Figure 6 shows the turbulence intensity at the MT-B offshore site. The average values for each wind speed bin of 1 m/s are shown separately for the warm and cold seasons. Despite a slight difference in trends, both the land and sea-sector winds showed greater turbulence intensity in the cold season than in the warm season.

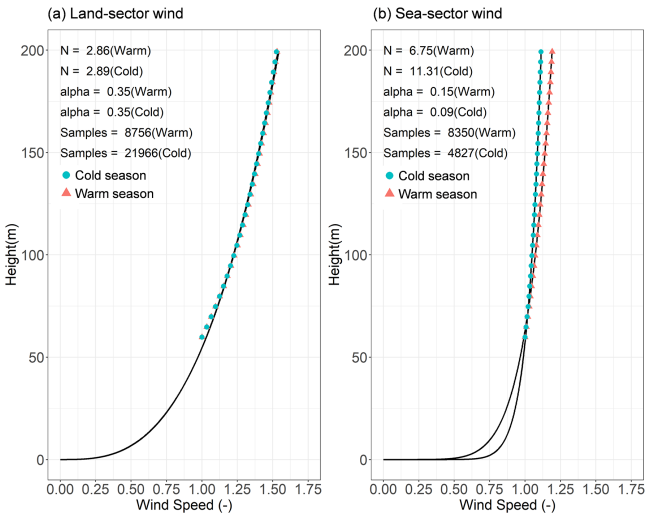

Fig. 5. Mean wind speed profiles for June 2017−May 2018 measured using LiDAR at site VL for (a) land-sector wind and (b) sea-sector wind. The wind speed is normalized by the wind speed at the lowest measurement height of 60 m. The solid line shows the power law fitted to the LiDAR measurements using the least squares method. The sector separation is based on the wind direction at the highest measurement height of 200 m.

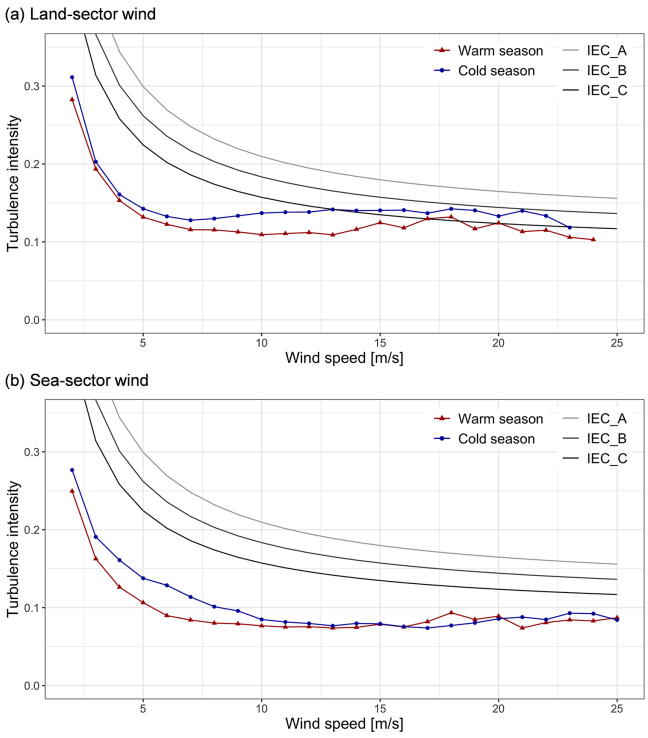

Fig. 6. Average turbulence intensity for each wind speed bin at the offshore site MT-B for (a) land-sector wind and (b) sea-sector wind. Red and blue lines denote the values for the warm season (September to March) and cold season (April to August), respectively.

For the land-sector wind, the turbulence intensity was high in the cold season, and this was probably due to the effect of westerly winter monsoon. For the sea-sector wind, the turbulence intensity tended to be high in the cold season in the low to medium wind speed range, with no such difference in the high wind range. This difference between wind speed ranges is due to atmospheric stability, which generally becomes neutral as the wind speed increases. In other words, because the atmospheric stability at

sea tends to be unstable in the cold season at the offshore site (as listed in Table 1), the turbulence intensity is greater than in the warm season at low to medium wind speed ranges.

4.4 Summary of discussion

By comparing the wind conditions in the warm and cold seasons in this section, it was found that the land–sea contrast of wind conditions was caused not only by mechanical but also thermodynamic factors such as seasonal variations in atmospheric stability. For monthly mean wind speeds (Fig. 2), the difference between onshore and offshore wind speed increased in the cold season, which was related to atmospheric stability over land and sea (shown in Fig. 4 and Table 1). This relationship can be explained as follows: As shown in Fig. 5, while the vertical wind speed shear over land is governed by mechanical effects and does not change throughout the year, the vertical shear over the sea greatly depends on atmospheric stability. In the cold season, the predominantly unstable conditions over the sea caused a lower vertical shear and higher wind speed in the lowest part of the atmospheric boundary layer. Thus, the wind speed differences between onshore and offshore sites increased during the cold season. Conversely, in the warm season, the prevailing neutral to stable conditions over the sea caused a greater wind shear and lower wind speed, and the wind speed difference became smaller between the onshore and offshore sites. These results suggest that the offshore wind resource assessment for a nearshore wind farm needs to carefully consider both the mechanical and thermodynamic effects caused by different surface conditions between land and sea.

5. Conclusions

This study investigated nearshore wind conditions, especially the land–sea contrast, in the coastal area of Mutsu-Ogawara, Aomori Prefecture, as a case study. Measurements from met masts and vertical LiDAR at land and sea sites in the Mutsu-Ogawara port were compared to determine the differences between onshore and offshore wind conditions. The main findings are summarized below.

First, wind conditions were largely different between onshore and offshore sites, which were 1.5 km apart. The mean wind speed at 55 m ASL at the offshore site was higher than that at the onshore site by up to 20% monthly and 12% annually. As for the turbulence intensity, the I_{ref} value for the land-sector wind at the offshore site was 37% lower than that at the onshore site. Thus, it is concluded that an offshore wind farm would have suitable wind conditions, even if placed very close to the coastline.

Next, the factors that cause the land–sea contrast of wind conditions were examined. While the vertical wind shear over the land is governed by surface roughness and canopy, and remains unchanged throughout the year, the vertical shear over the sea depends on atmospheric stability. The results suggest that the offshore wind resource assessment for a nearshore wind farm needs to carefully consider both the mechanical and thermodynamic effects caused by different surface conditions between land and sea.

The analyses in this study were mainly based on measurements from the met masts. However, the hub height of a typical offshore wind turbine can exceed 100 m. Thus, remote sensing devices, such as scanning LiDAR (Shimada et al. 2020) and floating LiDAR (Carbon Trust 2020), which can measure wind speeds for several hundred meters, are promising tools for surveying offshore wind conditions. For this reason, the New Energy and Industrial Technology Development Organization (NEDO) Fixed Offshore Wind Farm Development Support Project (Establishment of Offshore Wind Resource Assessment Method) (2019-22FY) is now underway to verify the practical effectiveness of these remote sensing devices through intensive meteorological observations at Mutsu-Ogawara. This study provides preliminary research on wind conditions prior to the NEDO project.

Acknowledgements

In this study, observation data from the buoy were made available by the managers, namely, the Mutsu Marine Laboratory, Japan Marine Science Foundation, which is under the jurisdiction of the Nuclear Safety Measures Division of the Aomori Crisis Management Bureau. The authors are grateful to Rokkasho Village Seawater Fisheries Cooperative for their support during the LiDAR observations. We also thank the students at the Air-Sea Laboratory of Kobe Graduate School for their technical support.

Edited by: H. Hashiguchi

Supplements

Supplementary figures: Wind rose figures at the offshore site MT-B for the period from April 2017 to March 2018.

References

Carbon Trust, 2020: Floating Wind Joint Industry Project – Phase 2 summary report. (Available online at: https://www.carbontrust.com/resources/floating-wind-joint-industry-project-phase-2-summary-report, accessed 5 September 2021).

Hsu, S.-A., 1988: *Coastal Meteorology, First Edition*. Academic Press, 260 pp.

International Electrotechnical Commission, 2019: Wind energy generation systems-Part 1: Design requirements, IEC 61400-1, Ed. 4.0.

Kanno, H., 1997: Classification of the Yamase (cold north-easterly wind around north-eastern Japan) based upon its air-mass vertical structures. *J. Meteor. Soc. Japan*, **75**, 1053−1071.

Kotake, N., S. Kameyama, Y. Kajiyama, and M. Enjo, 2016: Performance analysis of Mitsubishi Electric's wind lidar in the measurement campaign at European test sites. *Proc. WindEurope Summit*, Hamburg, Germany.

Nagai, N., H. Ogawa, A. Nakamura, Y. Suzuki, and K. Nukata, 2003: Occurrence characteristics of coastal wind energy based on observed data. *Proc. Coastal Eng. Japan Soc. Civ. Eng.*, **50**, 1306−1310.

Nassif, F. B., F. M. Pimenta, C. A. D'Aquino, A. T. Assireu, L. H. P. Garbossa, and J. C. Passos, 2020: Coastal wind measurements and power assessment using a LIDAR on a Pier. *Rev. Brasil. Meteor.*, **35**, 255−268.

Rodrigues, S., C. Restrepo, E. Kontos, R. Teixeira Pinto, and P. Bauer, 2015: Trends of offshore wind projects. *Renew. Sustain. Energy Rev.*, **49**, 1114−1135.

Sayigh, A., and D. Milborrow (eds.), 2020: *The Age of Wind Energy: Progress and Future Directions from a Global Perspective (Innovative renewable energy). First Edition*, Springer, 214 pp.

SethuRaman, S., and G. S. Raynor, 1980: Comparison of mean windspeeds and turbulence at a coastal site and offshore location. *J. Appl. Meteor. Climatol.*, **19**, 15−21.

Shima, S., 2016: Studies and activities in Japan Marine Science Foundation. *Japan. J. Health Phys.*, **51**, 251−253.

Shimada, S., Y. Takeyama, T. Kogaki, T. Ohsawa, and S. Nakamura, 2018: Investigation of the fetch effect using onshore and offshore vertical LiDAR devices. *Remote Sens.*, **10**, 1408.

Shimada, S., J. P. Goit, T. Ohsawa, T. Kogaki, and S. Nakamura, 2020: Coastal wind measurements using a single scanning LiDAR. *Remote Sens.*, **12**, 1347.

Manuscript received 27 July 2021, accepted 4 October 2021
SOLA: *https://www.jstage.jst.go.jp/browse/sola/*